ELSEVIER

Improved analysis of unidirectional composite delamination specimens

András Szekrényes [*]

Department of Applied Mechanics, Budapest University of Technology and Economics, P.O. Box 11, H-1521 Budapest, Hungary

Abstract

Generally, the delamination testing of composite specimens involves the analytical determination of the compliance and the energy release rate for the actual configuration. In this work an improved analysis for unidirectional composite delamination specimens is presented, which is based on the results of the last 30 years. The main goal of the present model is the improvement of the global mode decomposition method including four mechanical deformations apart from simple beam theory: Winkler–Pasternak foundation, transverse shear, Saint–Venant effect and crack tip shear deformation, respectively. These effects are investigated separately using a general loading scheme and at the final stage their results are superimposed. The derived model is applied to the mixed-mode I/II single-cantilever beam, the single-leg bending and the universal mixed-mode bending specimens. Beside the present solution three other ones are adopted to compare the results for the compliance and energy release rate of the mentioned specimens. Although the present model shows similar results to the most accurate finite element model, it is simpler and helps us to understand better the mechanisms of the delamination process.

1. Introduction

Within the scope of the linear elastic fracture mechanics (LEFM) the interlaminar fracture behavior of composite materials has been very intensively investigated in the literature. In this respect the most important quantity is the energy release rate (ERR), of which critical value must be exceeded in order to produce a unit of crack extension. In most cases for the common mode-I and mode-II beam-type specimens the ERR is determined through improved beam analysis. The double-cantilever beam (DCB) is a standard specimen for mode-I delamination testing. The elastic foundation was first applied by Kanninen and Popelar (1985) for the DCB specimen to model the deflection and rotation at the crack tip zone and to improve the formulae of the compliance and the ERR by simple beam theory. Williams (1989) extended this model for orthotropic materials, while Olsson (1992) completed the analysis of the DCB specimen with transverse shear and

---
[*] Tel.: +36 1 463 1170; fax: +36 1 463 3471.
E-mail address: szeki@mm.bme.hu

Saint–Venant (S–V) effects. The elastic foundation model was extended later for angle-ply laminate DCB coupons by Ozdil and Carlsson (1999a). For the mode-II end-notched flexure (ENF) delamination specimen improved beam analyses have been also performed. The first one was made by Carlsson et al. (1986), but only a little improvement was achieved. Ozdil et al. (1998) extended the Timoshenko beam theory for angle-ply laminate ENF specimens, while Ding and Kortschot (1999) introduced an elastic foundation model using tangential springs along the uncracked portion of the ENF coupon. In fact their model was too complicated and could not be applied directly. Later Wang and Qiao (2004a) presented a simpler and more practical solution for the ENF specimen, which had a similar form to that Williams (1989) provided for the DCB coupon. For mixed-mode I/II interlaminar fracture many configurations were developed (see the works by Davidson and Sundararaman (1996), Lai et al. (1996) and Sundararaman and Davidson (1997, 1998)). In this respect the standard mixed-mode bending (MMB) is the most universal tool. In the original papers of Crews and Reeder (1988) and Reeder and Crews (1990) a data reduction scheme based on elastic foundation and Timoshenko beam theory was developed. The single-cantilever beam (SCB), known as the mixed-mode end-loaded split (MMELS) specimen was applied among others by Hashemi et al. (1990a,b) and Reyes and Cantwell (2000) for experimental investigations. Also, beam-theory-based equations were applied for data reduction in these works. Improved expressions can also be obtained for the ERR using combined beam-theory-finite-element-based analysis. In this respect the work by Wang and Williams (1992) should be mentioned who presented corrections for mode-II ENF and ELS fracture specimens based on numerical calculations. Independently Bao et al. (1992) derived similar improvements for the DCB, mode-II ELS and SCB configurations.

In the case of mixed-mode I/II tests the mode-mixity analysis is an important issue. The so-called global method was developed by Williams (1988) based on simple beam theory. A different local approach was provided by Suo and Hutchinson (1990) using beam theory and integral equation methods. The latter was used to study several delamination specimens (Suo, 1990). Sundararaman and Davidson (1997, 1998) developed the crack tip element (CTE) analysis which was eventually equivalent to the local method. It should be mentioned that the local method is more accurate than the global one, because the latter is valid only in the case of midplane delamination and with same material properties of the upper and lower layers (Hutchinson and Suo, 1992; Bruno and Greco, 2001a; Zou et al., 2001, 2002). In few works (Zou et al., 2001; Bruno and Greco, 2001a) it has been shown, that if an appropriate kinematical plate model is used then the global method gives the same result as the local approach. Later, the local method was generalized for laminates with optional stacking sequence and multiple delaminations by Sheinman and Kardomateas (1997) and it was completed with shear effect using first-order shear deformable plate theory by Wang and Qiao (2004b,c). Bruno and Greco (2001a,b) also investigated the shear deformation effect on the ERR of delaminated plates. Notable contribution from shear–bending coupling was found, and it was shown that the shear effect improves only the mode-I component. Finally, the virtual crack-closure technique (VCCT) should be mentioned, which is widely accepted and applied for the computation of the ERR and mode decomposition in delaminated composite structures (Rybicki and Kanninen, 1977; Raju et al., 1988; Ducept et al., 1999).

The Winkler–Pasternak (W–P) elastic foundation is intensively applied by researchers to handle mainly dynamic (Rosa, 1995; Filipich and Rosales, 2002; Coşkun, 2003) and finite element problems (Alemdar and Gülkan, 1997; Omurtag and Kadıoğlu, 1998; Khazanovich, 2003). However, to the best of the author's knowledge it is not yet adopted for the beam analysis of fracture specimens. The two-parameter elastic foundation (Pasternak or Filonenko–Borodich) model assumes, that at the contact point between the beam and the foundation there are also moments, which are proportional to the angle of rotation. In our last work the Winkler-type elastic foundation and the result of the Timoshenko beam theory were extended for mixed-mode I/II (ELS and SLB) delamination specimens (Szekrényes and Uj, 2004). In the present work we analyse a more general loading scheme using the W–P foundation, Timoshenko beam theory, the theory of crack tip shear deformation (CTSD) analysis (Wang and Qiao, 2004a) and the S–V effect (Olsson, 1992). These effects are investigated separately but in the final stage the obtained results are superimposed. Finally, an improved scheme is developed, which is suitable to calculate the compliance, the mode-I and mode-II ERRs.

To demonstrate the accuracy of the developed model it is applied to the SCB, SLB and the MMB specimens, respectively and comparison is made with other analytical (Carlsson et al., 1986; Olsson, 1992; Bruno and Greco, 2001a) and numerical (Bao et al., 1992) solutions.

2. Beam analysis

In this section we adopt linear beam theories to obtain refined solution for the compliance and the ERR of midplane delaminated composite beams. The beams are assumed to have a linear elastic behavior and the model arms have the same mechanical properties. The W–P foundation analysis (Rosa, 1995; Szekrényes, 2005), Timoshenko beam theory (Washizu, 1968), S–V effect (Olsson, 1992) and the concept of CTSD analysis (Wang and Qiao, 2004a; Szekrényes, 2005) are utilized in our formulation. The total solution is obtained by the principle of superposition. Interaction among the former effects is not considered but in the last section some explanations will be available, which will show that the possible interactions can be ignored. Also, mode-mixity is performed by means of the global approach (Williams, 1988).

2.1. Winkler–Pasternak foundation analysis

The problem in Fig. 1 shows a delaminated beam is subjected to a general loading condition. In the uncracked region the two-parameter elastic foundation model captures the transverse elasticity. The

Fig. 1. Two-parameter elastic foundation model.

arms of the model are subjected to different loads. A detailed view at the crack tip is also shown at the bottom of Fig. 1. The linear springs are connected to the midplane of the upper and lower beam elements, while the moment in the torsional springs is proportional to the difference in the angle of rotations of the upper ($w_{u2}(x)$) and lower ($w_{l2}(x)$) beam elements. The potential energy of the system in Fig. 1 is

$$\Pi = \frac{1}{2} \int_{(l)} [I_{y2}^u E_{11} w_{u2}''(x)^2 + I_{y2}^l E_{11} w_{l2}''(x)^2$$
$$+ I_{y1}^u E_{11} w_{u1}''(x)^2 + I_{y1}^l E_{11} w_{l1}''(x)^2$$
$$+ k_e (w_{u2}(x) - w_{l2}(x))^2 + k_G (w_{u2}'(x) - w_{l2}'(x))^2] \mathrm{d}x$$
$$+ P_1 w_{u1}(-a) + P_2 w_{l1}(-a), \tag{1}$$

where I_{y2}^u, I_{y2}^l, I_{y1}^u and I_{y1}^l are the relevant second-order moments of inertia (refer to Fig. 1), E_{11} is the flexural modulus, k_e is the Winkler foundation parameter, k_G is the Pasternak foundation parameter and P_1 and P_2 are the external loads, respectively. The potential energy in the torsional springs is proportional to the square of the differences in the angle of rotations. The application of the minimum of the potential energy principle involves the following governing equations:

$$I_{y2}^l E_{11} \frac{\mathrm{d}^4 w_{l2}(x)}{\mathrm{d}x^4} - k_G \frac{\mathrm{d}^2 w_{l2}(x)}{\mathrm{d}x^2} + k_e w_{l2}(x)$$
$$= -k_G \frac{\mathrm{d}^2 w_{u2}(x)}{\mathrm{d}x^2} + k_e w_{u2}(x), \quad 0 \leqslant x \leqslant c,$$

$$I_{y2}^u E_{11} \frac{\mathrm{d}^4 w_{u2}(x)}{\mathrm{d}x^4} - k_G \frac{\mathrm{d}^2 w_{u2}(x)}{\mathrm{d}x^2} + k_e w_{u2}(x)$$
$$= -k_G \frac{\mathrm{d}^2 w_{l2}(x)}{\mathrm{d}x^2} + k_e w_{l2}(x), \quad 0 \leqslant x \leqslant c. \tag{2}$$

The definition of the foundation parameter k_e is (Ozdil and Carlsson (1999a):

$$k_e = \frac{b E_{33}}{h}. \tag{3}$$

The rotational foundation parameter cannot be so simply expressed. Generally, in the relevant literature the foundation parameters are varied within a wide range (Rosa, 1995; Alemdar and Gülkan, 1997; Coşkun, 2003), or only approximate expressions are given for the calculation of k_G (Omurtag and Kadıoğlu, 1998; Khazanovich, 2003). Some assumptions are required to determine the second foundation stiffness. The rearranged form of the governing equations is
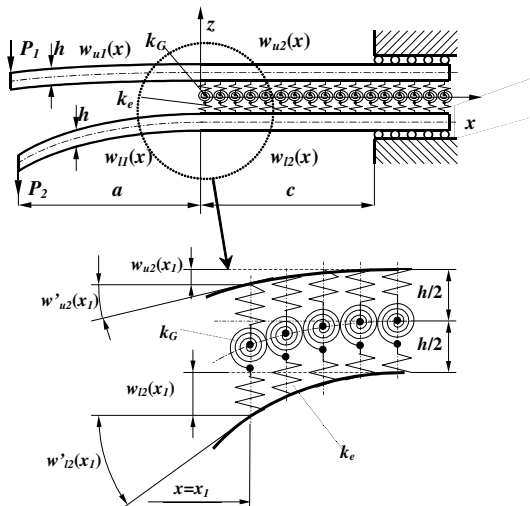
$$\frac{d^4 w_{l2}(x)}{dx^4} - 2\chi^4 \frac{d^2 w_{l2}(x)}{dx^2} + 4\eta^4 w_{l2}(x)$$
$$= -2\chi^4 \frac{d^2 w_{u2}(x)}{dx^2} + 4\eta^4 w_{u2}(x), \quad 0 \leqslant x \leqslant c,$$
$$\frac{d^4 w_{u2}(x)}{dx^4} - 2\chi^4 \frac{d^2 w_{u2}(x)}{dx^2} + 4\eta^4 w_{u2}(x)$$
$$= -2\chi^4 \frac{d^2 w_{l2}(x)}{dx^2} + 4\eta^4 w_{l2}(x), \quad 0 \leqslant x \leqslant c,$$
(4)

where η and χ will be defined later. Eq. (4) has three distinct solutions depending on which condition: $\chi^4 < 2^{1/2}\eta^2$, $\chi^4 = 2^{1/2}\eta^2$ or $\chi^4 > 2^{1/2}\eta^2$, respectively holds (Alemdar and Gülkan, 1997). It will be shown subsequently that in our case the last condition is involved. In this case the characteristic roots of Eq. (4) are:

$$m_{41} = \sqrt{\chi^4 - \sqrt{2}\eta^2},$$
$$m_{42} = \sqrt{\chi^4 + \sqrt{2}\eta^2}.$$
(5)

In the followings we assume that the rotational springs – similarly to the linear springs – depend on the through-thickness modulus (E_{33}). We adopt the following relation between χ and η:

$$\chi^4 = \omega 2^{1/2}\eta^2,$$
(6)

where $\omega > 1$ and will be determined based on finite element (FE) calculations. The solutions of the un-cracked part are given by

$$w_{l2}(x) = c_1 + c_2 x + c_3 x^2 + c_4 x^3 + [c_5 \cosh(m_{41}x) + c_6 \sinh(m_{41}x)] \cosh(m_{42}x) + [c_7 \cosh(m_{41}x) + c_8 \sinh(m_{41}x)] \sinh(m_{42}x),$$
$$0 \leqslant x \leqslant c,$$
$$w_{u2}(x) = c_1 + c_2 x + c_3 x^2 + c_4 x^3 - [c_5 \cosh(m_{41}x) + c_6 \sinh(m_{41}x)] \cosh(m_{42}x) - [c_7 \cosh(m_{41}x) + c_8 \sinh(m_{41}x)] \sinh(m_{42}x),$$
$$0 \leqslant x \leqslant c.$$
(7)

The deflection functions of the upper and lower model arms (Fig. 1) can be expressed in the usual way using Euler–Bernoulli beam theory. Using the theorem of parallel axes the second-order moments of inertia of the cracked and uncracked portions of the model in Fig. 1 are $I_{y2}^u = I_{y2}^l = h^3 b/3$ and $I_{y1}^u = I_{y1}^l = h^3 b/12$, respectively, where in the calculation of I_{y2}^u and I_{y2}^l it was considered that the reference plane coincides with the x–y plane of the model depicted in Fig. 1. The same method was applied by

Davidson and Sundararaman (1996) and Sundararaman and Davidson (1998). This condition assumes strain compatibility along the interface, which is assumed not to be violated by the elastic foundation. The coefficients, η and χ may be expressed by using Eqs. (2)–(4) and (6):

$$\eta = \left(\frac{k_e}{4 I_{y2}^u E_{11}}\right)^{\frac{1}{4}} = \left(\frac{3}{4}\right)^{\frac{1}{4}} \frac{1}{h} \left(\frac{E_{33}}{E_{11}}\right)^{\frac{1}{4}},$$
$$\chi = \left(\frac{k_G}{2 I_{y2}^u E_{11}}\right)^{\frac{1}{4}} = \omega^{\frac{1}{4}} \left(\frac{3}{2}\right)^{\frac{1}{8}} \frac{1}{h^{\frac{1}{2}}} \left(\frac{E_{33}}{E_{11}}\right)^{\frac{1}{8}}.$$
(8)

The constants (c_1–c_8) in Eq. (7) and further four unknown constants (c_9–c_{12}) in the deflection functions of the upper and lower model arms can be obtained by using the usual boundary and matching conditions. However, the following matching conditions are important to highlight:

$$w_{u1}''(0) = 4w_{u2}''(0), \quad w_{l1}''(0) = 4w_{l2}''(0),$$
$$w_{u1}'''(0) = 4w_{u2}'''(0), \quad w_{l1}'''(0) = 4w_{l2}'''(0).$$
(9)

It is noteworthy that the theorem of parallel axes should be considered when we match the second and third derivative of the relevant deflection functions in Eq. (9). We are interested to find the compliance of each arm, that can be obtained by taking the deflections $w_{u1}(x)$, $w_{l1}(x)$ at the position of $x = -a$ and dividing them by the external loads, P_1 and P_2, respectively. Meaningful simplifications can be achieved by assuming that the length of the uncracked region, c is much larger than half of the specimen thickness, h. Note that the constant parameters, c_1–c_{12} are extremely complicated, therefore they are not detailed here. Utilizing Eq. (8) the compliance of the upper arm becomes:

$$C_{EB,WP,1} = \frac{7a^3 + L^3}{2bh^3 E_{11}} + \frac{(L^3 - a^3)P_2}{2bh^3 E_{11} P_1} + \frac{a^3(P_1 - P_2)}{2bh^3 E_{11} P_1} f_{W1},$$
(10)

where $L = a + c$ is the full length of the model in Fig. 1. Furthermore:

$$f_{W1} = 2.71 \left(\frac{h}{a}\right) \left(\frac{E_{11}}{E_{33}}\right)^{\frac{1}{4}} \phi^{\frac{1}{2}} + 2.45 \left(\frac{h}{a}\right)^2 \left(\frac{E_{11}}{E_{33}}\right)^{\frac{1}{2}} \phi$$
$$+ 1.11 \left(\frac{h}{a}\right)^3 \left(\frac{E_{11}}{E_{33}}\right)^{\frac{3}{4}} \phi^{\frac{1}{2}},$$
(11)

where $\phi = 1 + \omega$. The first two terms in Eq. (10) are the result of the Euler–Bernoulli beam theory, while

the third one is the correction based on the two-parameter elastic foundation. A similar expression may be obtained for the lower arm. The ERR for the upper arm may be obtained by using the following equation (Anderson, 2005):

$$G_{EB,WP,1} = \frac{P_1^2}{2b} \frac{dC_{EB,WP,1}}{da}. \tag{12}$$

Thus, we may obtain:

$$G_{EB,WP,1} = \frac{21P_1^2a^2}{4b^2h^3E_{11}} - \frac{3P_1P_2a^2}{4b^2h^3E_{11}} + \frac{P_1(P_1 - P_2)a^2}{4b^2h^3E_{11}}f_{W2}, \tag{13}$$

where

$$f_{W2} = 5.42\left(\frac{h}{a}\right)\left(\frac{E_{11}}{E_{33}}\right)^{\frac{1}{4}}\phi^{\frac{1}{2}} + 2.45\left(\frac{h}{a}\right)^2\left(\frac{E_{11}}{E_{33}}\right)^{\frac{1}{2}}\phi. \tag{14}$$

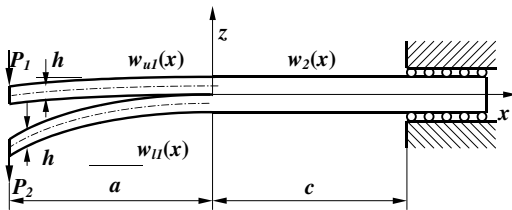The ERR for the lower arm of the model in Fig. 1 can be calculated similarly.

Fig. 2. A general loading scheme for Timoshenko beam theory.

2.2. Timoshenko beam theory

Fig. 2 shows a delaminated beam loaded by different concentrated forces at the end of both arms and the beam has a clamped end. The effect of transverse shear was analysed in our last work (Szekrényes and Uj, 2004). The analysis resulted in the following compliance and ERR corrections:

$$C_{TIM,1} = \frac{L(P_1 + P_2) + a(P_1 - P_2)}{2bhkG_{13}P_1}, \tag{15}$$

where G_{13} is the shear modulus in the x–z plane, furthermore the ERR is

$$G_{TIM,1} = \frac{P_1(P_1 - P_2)}{4b^2hkG_{13}}, \tag{16}$$

where $k = 5/6$ is the shear correction factor. For the lower arm similar expressions can be derived.

2.3. Saint–Venant effect

Olsson (1992) considered the problem of S–V effect in the compliance analysis of the mode-I DCB specimen. In this section we adopt the same theory. The S–V effect represents a rotational angle at the crack tip or at the clamped end of the model. In Fig. 3 three cases are compiled. Fig. 3a shows the deformation of the crack tip under pure mode-I condition. In this case the strain compatibility condition is satisfied, hence the S–V effect should be considered. In contrast, focusing our attention on Fig. 3b we may observe that the
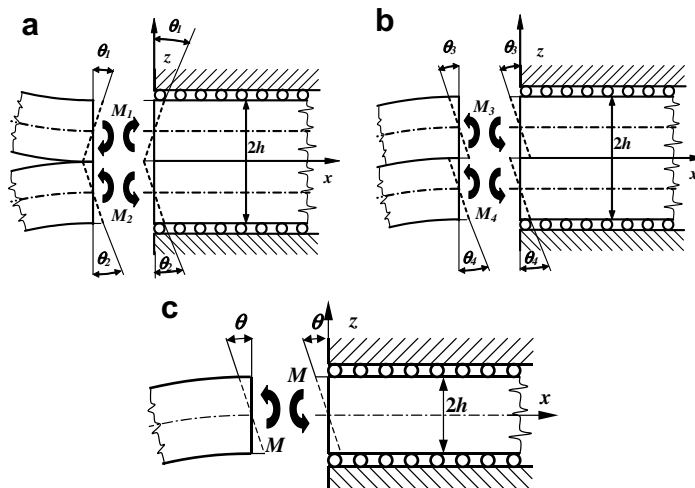

Fig. 3. Saint–Venant effect under pure mode-I (a) and pure mode-II (b). Saint–Venant effect at the clamped end (c).
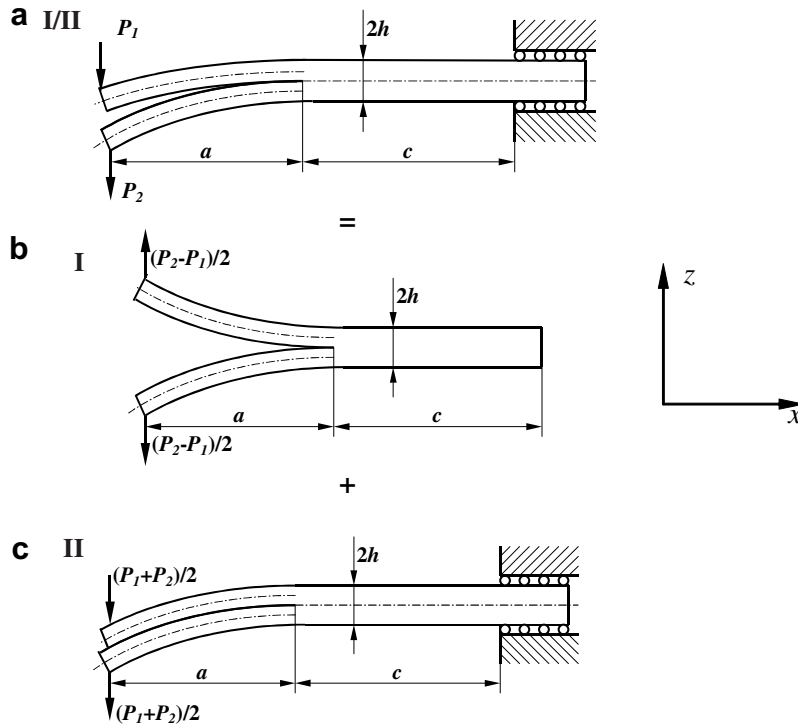
Fig. 4. Application of the principle of superposition.

S–V effect must vanish if the pure mode-II condition is involved. In this case the rotational angles would induce opposite axial displacements at the crack tip, which is physically not possible. Finally, Fig. 3c shows the clamped end of the uncracked part of the model, where the S–V effect also takes place. Therefore, in the sequel we discuss only the pure mode-I condition and the case of the clamped end. The mixed-mode I/II problem can be separated into the unique mode-I and mode-II problems using the principle of superposition (refer to Fig. 4). We note that in accordance with strength of materials analysis there are zero axial displacements at the clamped end. The present formulation is an attempt to capture better the deformation at the clamped end.

According to Olsson's analysis the derivative of the strain energy in the coordinate system in Fig. 3 is bounded by the following inequality:

$$\frac{\partial U}{\partial x} \leqslant 2 \frac{\partial U}{\partial x}\bigg|_0 e^{-\frac{2x}{\kappa}}, \quad \kappa = \frac{h}{2\pi}\left(\frac{E_{11}}{G_{13}}\right)^{\frac{1}{2}}, \tag{17}$$

where U is the strain energy, κ is the characteristic decay length in the material.

2.3.1. Saint–Venant effect at the crack tip

In the followings we investigate the mode-I part of the problem (Fig. 4b), furthermore only the upper half of the model is considered. In the case of slender beams under bending the derivative of the strain energy per unit length can be calculated as

$$\left(\frac{\partial U}{\partial x}\right)_1\bigg|_0 = \frac{1}{2}I_{y1}^u E_{11}(w''|_0)^2 = \frac{1}{2}\frac{M_1^2}{I_{y1}^u E_{11}} = \frac{6M_1^2}{bh^3 E_{11}}, \tag{18}$$

where I_{y1}^u is identical to that mentioned in Section 2.1. The moments, M_1 and M_2 are (refer to Fig. 4b):

$$M_1 = \frac{(P_1 - P_2)a}{2}, \quad M_2 = \frac{(P_2 - P_1)a}{2}. \tag{19}$$

For M_3 and M_4 in Fig. 3 refer to Fig. 4c. From Eqs. (17) and (18) the strain energy ahead of the crack tip is

$$U_1 \leqslant \int_0^\infty 2\left(\frac{\partial U}{\partial x}\right)_1\bigg|_0 e^{-\frac{2x}{\kappa}} dx$$
$$= \frac{12M_1^2}{bh^3 E_{11}} \int_0^\infty e^{-\frac{2x}{\kappa}} dx \Rightarrow U_1 \leqslant \frac{6M_1^2 \kappa}{bh^3 E_{11}}. \tag{20}$$

Let us consider the lower sign in Eq. (20). Using Castigliano's second theorem and Eq. (19) we obtain the rotational angles at $x = 0$:

$$\theta_1 = \frac{\partial U_1}{\partial M_1} = \frac{12 M_1 \kappa}{bh^3 E_{11}} = \frac{6(P_1 - P_2)a\kappa}{bh^3 E_{11}}. \qquad (21)$$

The displacement at the end of the model arm is (see Fig. 5)

$$\delta_1 = \theta_1 a = \frac{6(P_1 - P_2)a^2 \kappa}{bh^3 E_{11}}. \qquad (22)$$

Substituting κ (the second in Eq. (17)) into Eq. (22) we obtain:

$$C_{SV,1} = \frac{\delta_1}{P_1} = \frac{3}{\pi} \frac{(P_1 - P_2)a^2}{bh^2 E_{11} P_1} \left(\frac{E_{11}}{G_{13}} \right)^{\frac{1}{2}}. \qquad (23)$$

the application of Eq. (12) results in the ERR as

$$G_{SV,1} = \frac{P_1(P_1 - P_2)a^2}{4b^2 h^3 E_{11}} f_{SV}, \qquad (24)$$

where

$$f_{SV} = \frac{12}{\pi} \left(\frac{h}{a} \right) \left(\frac{E_{11}}{G_{13}} \right)^{\frac{1}{2}}. \qquad (25)$$

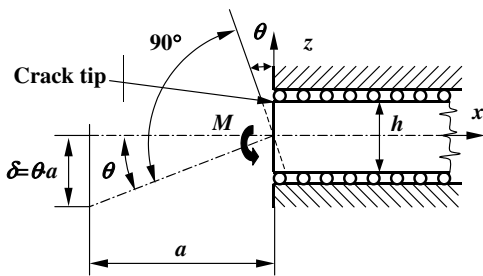For the lower half of the problem similar expressions can be obtained.

Fig. 5. Deformation of the crack tip due to Saint–Venant effect.

2.3.2. Saint–Venant effect at the clamped end

A similar analysis at the clamped end of the model (see Fig. 3c) gives:

$$C_{SV} = \frac{3}{\pi} \frac{L^2}{2bh^2 E_{11}} \left(\frac{E_{11}}{G_{13}} \right)^{\frac{1}{2}}, \qquad (26)$$

where $L = a + c$ is the full length of the model. As it can be seen, in this case there is no contribution to the ERR.

2.4. Crack tip shear deformation analysis

Wang and Qiao (2004a) performed an improved beam analysis for the mode-II ENF coupon. Their solution can be easily extended for mixed-mode I/II specimens. Let us consider the problem in Fig. 6. Based on the strength of materials analysis the shear stresses in the upper and lower arms of the model are:

$$\tau_{01} = \frac{3}{2} \frac{P_1}{bh}, \qquad \tau_{02} = \frac{3}{2} \frac{P_2}{bh}. \qquad (27)$$

We consider the shear stresses in Eq. (27) as shear tractions and the effect of the concentrated forces, P_1 and P_2 is not included in the analysis (they have already been considered in Sections 2.1 and 2.2). In contrast with Wang and Qiao (2004a) in the present analysis we assume that the shear tractions act along the midplane of the upper and lower arms and do not between crack faces. The relationships between the section forces and stresses of the uncracked region are:

$$\frac{dN_{u2}}{dx} = b\tau_{u2}, \quad \frac{dN_{l2}}{dx} = b\tau_{l2}, \quad \frac{dM_{u2}}{dx} = -\frac{h}{2} b\tau_{u2},$$

$$\frac{dM_{l2}}{dx} = -\frac{h}{2} b\tau_{l2}, \qquad (28)$$

where N is the normal force and M is the bending moment, respectively. The relationship between the deflections and the bending moments are:
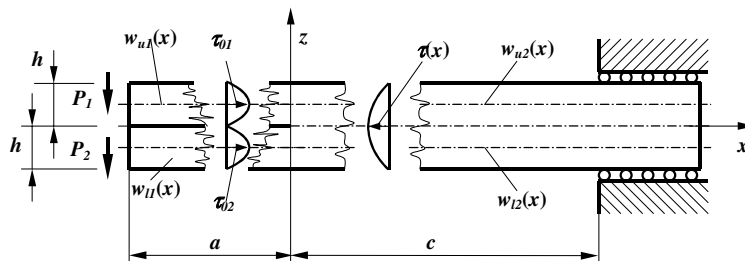

Fig. 6. Loading scheme for the crack tip shear deformation analysis.

$$\frac{\mathrm{d}^2 w_{u2}}{\mathrm{d}x^2} = \frac{-M_{u2}}{I_{y2}^u E_{11}}, \quad \frac{\mathrm{d}^2 w_{l2}}{\mathrm{d}x^2} = \frac{-M_{l2}}{I_{y2}^l E_{11}}, \tag{29}$$

where I_{y2}^u and I_{y2}^l are the same moments of inertia as mentioned in Section 2.1. The longitudinal displacement at the neutral plane of the uncracked portion ($0 \leqslant x \leqslant c$) can be written as

$$u_{u2}(x) = -\int \frac{N_{u2}}{bhE_{11}} \mathrm{d}x + K_1 \tau_{u2} - \frac{h}{2} \frac{\mathrm{d}w_{u2}}{\mathrm{d}x}, \tag{30}$$

$$u_{l2}(x) = \int \frac{N_{l2}}{bhE_{11}} \mathrm{d}x - K_2 \tau_{l2} + \frac{h}{2} \frac{\mathrm{d}w_{l2}}{\mathrm{d}x}, \tag{31}$$

where K_1 and K_2 are the shear compliances and we will define them later. Along the interface of the upper and lower beam elements of the uncracked region the axial displacements should be identical, i.e. strain compatibility is required and the relative displacement is zero:

$$u_{u2}(x) - u_{l2}(x) = 0. \tag{32}$$

Substituting Eqs. (30) and (31) into (32) and differentiating the resulting expression twice we have:

$$-\frac{1}{bhE_{11}} \left[\frac{\mathrm{d}N_{u2}}{\mathrm{d}x} + \frac{\mathrm{d}N_{l2}}{\mathrm{d}x} \right] + K_1 \frac{\mathrm{d}^2 \tau_{u2}}{\mathrm{d}x^2} + K_2 \frac{\mathrm{d}^2 \tau_{l2}}{\mathrm{d}x^2}$$
$$- \frac{h}{2} \left[\frac{\mathrm{d}^3 w_{u2}}{\mathrm{d}x^3} + \frac{\mathrm{d}^3 w_{l2}}{\mathrm{d}x^3} \right] = 0. \tag{33}$$

In accordance with Wang and Qiao (2004a) the shear compliances are $K_1 = K_2 = h/3G_{13}$. Combining Eqs. (28), (29) and (33) and recognizing that at the interface the shear stresses are equal ($\tau_{u2} = \tau_{l2} = \tau$), the following governing equation can be obtained:

$$\frac{\mathrm{d}^2 \tau}{\mathrm{d}x^2} - \rho^2 \tau = 0, \quad \rho = \left(\frac{21G_{13}}{4E_{11}h^2} \right)^{\frac{1}{2}}. \tag{34}$$

The solution of Eq. (34) is

$$\tau(x) = f_1 \mathrm{e}^{-\rho x} + f_2 \mathrm{e}^{\rho x}. \tag{35}$$

Referring to Wang and Qiao (2004a) the second term in Eq. (35) can be neglected. On the other hand the longitudinal forces must vanish along the whole length of the model, i.e.:

$$\int_{-a}^{0} (\tau_{01} + \tau_{02}) bh \, \mathrm{d}x - \int_{0}^{c} f_1 \mathrm{e}^{-\rho x} b \cdot 2h \cdot \mathrm{d}x = 0. \tag{36}$$

Assuming that $\mathrm{e}^{-\rho c} \cong 0$ if $c \gg h$ we obtain from Eqs. (27), (35) and (36) the following solution:

$$\tau(x) = -\frac{3}{4} \frac{P_1 + P_2}{bh} \rho \cdot a \mathrm{e}^{-\rho x}. \tag{37}$$

In the sequel we analyse only the upper half of the model. The bending moment function in the uncracked region using Eq. (28) is

$$M_{u2}(x) = -\frac{h}{2} \left[\int \frac{3}{4} \frac{P_1 + P_2}{bh} \rho \cdot a \mathrm{e}^{-\rho x} b \cdot \mathrm{d}x \right]$$
$$= \frac{3}{8} (P_1 + P_2) a \mathrm{e}^{-\rho x}. \tag{38}$$

Using Eqs. (29) and (38) the deflection function of the uncracked part becomes:

$$w_{u2}(x) = -\frac{3}{8} \frac{(P_1 + P_2)a}{I_{y2}^u E_{11} \rho^2} \mathrm{e}^{-\rho x} + g_1 x + g_2. \tag{39}$$

Since the shear stresses act along the neutral plane of the upper and lower model arms they do not cause bending moment, consequently they are simple linear functions. Using the boundary conditions depicted in Fig. 6 and matching the deflections and their derivates at $x = 0$ we may obtain the compliance of the upper arm of the model after some simplifications (Wang and Qiao, 2004a):

$$C_{\mathrm{SH,1}} = \frac{w_{u1}(-a)}{P_1} = \frac{(P_1 + P_2)a^3}{2P_1 bh^3 E_{11}} f_{\mathrm{SH1}}, \tag{40}$$

where

$$f_{\mathrm{SH},1} = 0.98 \left(\frac{h}{a} \right) \left(\frac{E_{11}}{G_{13}} \right)^{\frac{1}{2}} + 0.43 \left(\frac{h}{a} \right)^2 \left(\frac{E_{11}}{G_{13}} \right). \tag{41}$$

The ERR for the upper arm by using Eq. (12) is

$$G_{\mathrm{SH,1}} = \frac{P_1(P_1 + P_2)a^3}{2b^2 h^3 E_{11}} f_{\mathrm{SH2}}, \tag{42}$$

where

$$f_{\mathrm{SH2}} = 1.96 \left(\frac{h}{a} \right) \left(\frac{E_{11}}{G_{13}} \right)^{\frac{1}{2}} + 0.43 \left(\frac{h}{a} \right)^2 \left(\frac{E_{11}}{G_{13}} \right). \tag{43}$$

The solution can be obtained also for the lower half of the problem; however it is noteworthy that the analysis shows that the deflection functions of the upper and lower beam elements are identical.

2.5. Mode-mixity analysis – global method

Let us consider the problem in Fig. 7a. We superimpose the results of the elastic foundation, transverse shear analysis, S–V and CTSD effects, respectively. The compliance of the upper arm of the model (Fig. 7a) by summarizing Eqs. (10), (15), (23) and (40) is
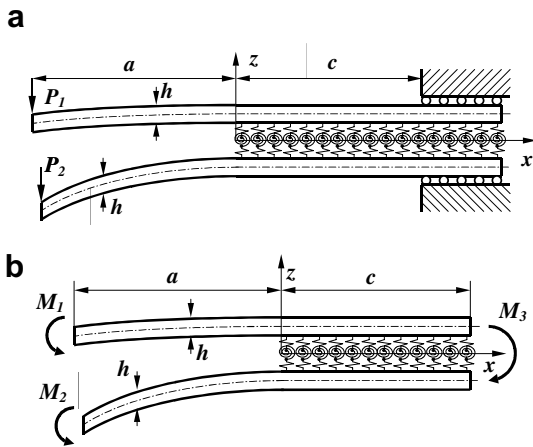
a

b

Fig. 7. Reduction scheme for mixed-mode partitioning. Original problem (a). Reduced problem (b).

$$C_1 = \frac{7a^3 + L^3}{2bh^3 E_{11}} + \frac{(L^3 - a^3)P_2}{2bh^3 E_{11} P_1}$$
$$+ \frac{L(P_1 + P_2) + a(P_1 - P_2)}{2bhkG_{13}P_1}$$
$$+ \frac{a^3(P_1 - P_2)}{2bh^3 E_{11} P_1}\left(f_{W1} + \frac{f_{SV}}{2}\right) + \frac{a^3(P_1 + P_2)}{2bh^3 E_{11} P_1} f_{SH1},$$

$$(44)$$

where f_{W1} is the correction from two-parameter elastic foundation analysis, f_{SV} is the correction from S–V effect and f_{SH1} is from CTSD analysis, respectively. Note that the S–V effect is considered only at the crack tip. The ERR for the upper arm by summarizing Eqs. (13), (16), (24) and (42) is

$$G_1 = \frac{21 P_1^2 a^2}{4b^2 h^3 E_{11}} - \frac{3 P_1 P_2 a^2}{4b^2 h^3 E_{11}}$$
$$+ \frac{P_1(P_1 - P_2)a^2}{4b^2 h^3 E_{11}}(f_{W2} + f_T + f_{SV})$$
$$+ \frac{P_1(P_1 + P_2)a^2}{4b^2 h^3 E_{11}} f_{SH2},$$

$$(45)$$

where f_T is defined as

$$f_T = \frac{1}{k}\left(\frac{h}{a}\right)^2 \left(\frac{E_{11}}{G_{13}}\right).$$

$$(46)$$

According to Fig. 7 we reduce problem (a) into problem (b), where $M_1 = P_1 a$, $M_2 = P_2 a$, and $M_3 = M_1 + M_2$ are bending moments at the crack tip. The total ERR (including Eq. (45) and the relevant solution for the lower arm) can be transformed as

Following Williams' global mode decomposition method (Williams, 1988; Ducept et al., 1999) the mode-I and mode-II ERR components become:

$$G_I = \frac{M_I^2(12 + f_{W2} + f_T + f_{SV})}{b^2 h^3 E_{11}},$$
$$G_{II} = \frac{M_{II}^2(9 + f_{SH2})}{b^2 h^3 E_{11}},$$

$$(48)$$

where the mode-I and mode-II bending moments (Williams, 1988; Ducept et al., 1999) are:

$$M_I = (M_1 - M_2)/2, \quad M_{II} = (M_1 + M_2)/2. \quad (49)$$

According to the first of Eq. (48) the W–P foundation, transverse shear and the S–V effect contributes only to the mode-I component. The first is obvious, since the two-parameter elastic foundation incorporates the differences between the vertical displacements and the angle of rotations of the upper and lower beam elements. Under mode-II these are equal to zero. Considering the transverse shear effect the conclusion may be explained by the fact that under pure mode-II the cracked and uncracked portions have the same shear compliances. This was supported also by Ozdil and Carlsson (1999a) and Wang and Qiao (2004a). It has already been discussed why the S–V effect contributes only to the mode-I component. On the other hand the CTSD improves only the mode-II component according to the second of Eq. (48).

2.6. Compliance calculation

We derive a general expression based on a superposition analysis, which can be applied to calculate the compliance for a symmetrically delaminated unidirectional beam under general mixed-mode I/II loading condition. The method is the generalization of that presented by Ozdil and Carlsson (1999b) for the MMB test rig. In a general form the mode-I and mode-II bending moments in Eq. (49) are:

$$M_I = P \cdot f_I \cdot a^{\#}, \quad M_{II} = P \cdot f_{II} \cdot a^{\#}, \quad (50)$$

where P is the external load, f_I and f_{II} are related to geometrical parameters of the system and $a^{\#}$ is the characteristic length (in each case may be related to the crack length). It is noteworthy that in some specimens the characteristic length is the length of

$$G_T = \frac{21(M_1^2 + M_2^2) - 6M_1 M_2 + (M_1 - M_2)^2(f_{W2} + f_T + f_{SV}) + (M_1 + M_2)^2 f_{SH2}}{4b^2 h^3 E_{11}}.$$

$$(47)$$

the uncracked portion (e.g.: the ONF and OLB specimens (Szekrényes and Uj, 2005, 2007)). Actually, it is helpful to use concentrated forces instead of the moments:

$$P_I = P \cdot f_I, \quad P_{II} = P \cdot f_{II}, \tag{51}$$

i.e., $M_I = P_I a^\#$ and $M_{II} = P_{II} a^\#$. We note that Eq. (44) is applicable only in particular circumstances, namely when the external loads act at the end of the model arms. Although the extension of the model (Eq. (44)), for example to the ELS, SCB and DCB specimens is relatively simple, the application, for instance to the SLB and MMB specimens is not so trivial. Hence, a more general scheme is preferred. Based on the present chapter the compliance of unidirectional composite beams with midplane delamination may be written as

$$C = C_{EB} + C_{TIM} + C_{W1} + C_{SV1} + C_{SH1} + C_{SV}, \tag{52}$$

where C_{EB} is the result of Euler–Bernoulli beam theory, C_{TIM} is the contribution of transverse shear deformation, C_{W1} is the effect of the W–P foundation, C_{SV1} is from the S–V effect at the crack tip, C_{SH1} accounts for the CTSD and C_{SV} considers the S–V effect at the clamped end, respectively. The determination of the first two terms requires a unique analysis. Usually, these two terms may be determined by following the way shown by Ozdil et al. (1998). On the other hand C_{SV} (Eq. (26)) is a simple additive term. Considering the other three terms it has been shown that the W–P foundation and the S–V effect at the crack tip contributes to the mode-I, while the CTSD improves the mode-II component. We assume that the deflection at the point of load application (δ) is equal to the sum of the displacements related to the mode-I and mode-II effects:

$$\delta = \delta_{EB} + \delta_{TIM} + f_I \delta_I + f_{II} \delta_{II} + C_{SV} P, \tag{53}$$

where f_I and f_{II} are the same as those mentioned in Eq. (50). The compliance corrections related to the mode-I and mode-II effects may be expressed as

$$C_I = \frac{\delta_I}{P_I} = C_{W1} + C_{SV1}, \quad C_{II} = \frac{\delta_{II}}{P_{II}} = C_{SH1}. \tag{54}$$

The combination of Eqs. (51) and (54) with Eq. (53) leads to the followings:

$$\delta = \delta_{EB} + \delta_{TIM} + C_I f_I^2 P + C_{II} f_{II}^2 P + C_{SV} P,$$
$$C = C_{EB} + C_{TIM} + C_I f_I^2 + C_{II} f_{II}^2 + C_{SV}. \tag{55}$$

The compliance related to the mode-I loading (C_I) can be obtained by substituting $P_1 = P$ and $P_2 = -P$ into Eq. (44) and the one for the lower model arm. Similarly, the compliance related to the mode-II loading (C_{II}) can be obtained by substituting $P_1 = P_2 = -P/2$ into the same equations. The former is the case of the mode-I DCB specimen, while the latter is that of the mode-II ELS specimen. In other words the solution is obtained as the superposition of the models of these specimens. Using the geometrical factors, f_I and f_{II} the compliance can be transformed to the point of load application even if the load does not act at the model end, for example in the SLB and MMB specimens (see later). Therefore, the terms C_{W1}, C_{SV1} and C_{SH1} may be calculated by achieving the former substitutions into Eq. (44) and the one for the lower arm and comparing to Eq. (55), this calculation gives:

$$C_{W1} = \frac{2a^3}{bh^3 E_{11}} f_{W1}, \quad C_{SV1} = \frac{2a^3}{bh^3 E_{11}} \frac{f_{SV}}{2},$$
$$C_{SH1} = \frac{2a^3}{bh^3 E_{11}} f_{SH1}. \tag{56}$$

Combining Eq. (54), the second of (55) and Eq. (56) the following expression is obtained:

$$C = C_{EB} + C_{TIM} + \frac{2f_I^2 a^3}{bh^3 E_{11}} \left(f_{W1} + \frac{f_{SV}}{2} \right)$$
$$+ \frac{2f_{II}^2 a^3}{bh^3 E_{11}} f_{SH1} + C_{SV}, \tag{57}$$

where f_{W1} is given by Eq. (11), f_{SV} is given by Eq. (25), f_{SH1} is defined by Eq. (41) and C_{SV} is given by Eq. (26). Finally, there is now only one unknown parameter, ω, (in Eq. (6)) of which determination is detailed in the following.

2.7. Determination of the coefficient of the Pasternak foundation

We assumed that the torsional springs in the two-parameter elastic foundation (see Fig. 1) are related to the through-thickness (E_{33}) modulus of the specimen. If we consider a spring with stiffness of infinity this is equivalent to the case, when $E_{33} = \infty$. If this is the case there is no relative vertical displacement between the upper and lower beam elements of the uncracked region. Moreover, in this case the relative angle of rotation of the upper and lower beam elements is also equal to zero, and consequently even the potential energy in the torsional springs becomes zero (Eq. (1)). This indicates that the initial assumption is right. In order to determine the unknown parameter (ω) the FE method is used.

First of all the effect of two-parameter elastic foundation should be isolated within the model. In other words the transverse shear, S–V and CTSD effects, which are related to the shear modulus of the model should be eliminated. This may be achieved if we construct a model, wherein the shear modulus tends to infinity, i.e.: $G_{13} \rightarrow \infty$. If this is the case the terms in Eq. (57), which are related to the shear modulus G_{13} vanish, since the related corrections (C_{TIM}, f_{SV}, f_{SH1}, C_{SV}) become zero. It may be assumed that the remaining correction can be completely related to the W–P foundation (f_{W1}).

To determine ω the simplest way is to consider the FE model of a DCB specimen, in which the shear modulus is $G_{13} = 100\,000$ GPa. The compliance and the ERR of the FE model of the DCB specimen may be written as (Wang and Williams, 1992)

$$C_{\text{FE}}^{\text{DCB}} = \frac{8(a + \xi h)^3}{bh^3 E_{11}}, \quad G_{\text{I,FE}}^{\text{DCB}} = \frac{12P^2(a + \xi h)^2}{b^2 h^3 E_{11}}, \quad (58)$$

where ξ is the correction from the FE analysis if $G_{13} = 100\,000$ GPa. Rearranging the first of Eq. (58) ξ is equal to:

$$\xi = \sqrt[3]{\frac{C_{\text{FE}}^{\text{DCB}} b E_{11}}{8}} - \frac{a}{h}, \quad (59)$$

where it was assumed that the correction ξ does not depend on the crack length, it depends only on material properties.

For the application of the analytical model (Eq. (48)) we need the bending moments at the crack tip of the DCB specimen, which are: $M_1 = -M_2 = Pa$. Furthermore, Eq. (49) yields that $M_{\text{I}} = Pa$ and $M_{\text{II}} = 0$ and from Eq. (50) that $f_{\text{I}} = 1$ and $f_{\text{II}} = 0$. Incorporating Eq. (48) the ERR of the DCB model including only the effect of the two-parameter elastic foundation is:

$$G_{\text{I,WP}}^{\text{DCB}} = \frac{12P^2 a^3}{b^2 h^3 E_{11}} + \frac{P^2 a^2}{b^2 h^3 E_{11}} \left[5.42 \left(\frac{h}{a}\right) \left(\frac{E_{11}}{E_{33}}\right)^{\frac{1}{4}} \phi^{\frac{1}{2}} \right.$$
$$\left. + 2.45 \left(\frac{h}{a}\right)^2 \left(\frac{E_{11}}{E_{33}}\right)^{\frac{1}{2}} \phi \right], \quad (60)$$

where $\phi = 1 + \omega$. The FE analysis was performed by using the COSMOS/M 2.0 package. The model of the DCB specimen was meshed with linear elastic PLANE2D elements under plane stress state. The upper and lower arms of the model were subjected to concentrated forces equal to unity. The displacements of the arms were used to calculate the compli-

ance of the model, the value of ξ was determined from Eq. (59). The next step was to compare the second of Eq. (58) with Eq. (60). In Eq. (60) ω was chosen in order to reach the best agreement with the second of Eq. (58), i.e. with the FE solution, where G_{13} is equal to $100\,000$ GPa. A large amount of FE analysis on models of the DCB specimen with different geometrical and material properties were performed in the crack length range of $a = 30$–100 mm. The results are summarized in Table A1 (Appendix). In all the cases it was found that if we choose $\omega = 2.5$ then the agreement between the FE and analytical solution is excellent. Also, this result ($\omega > 1$) justifies why Eq. (7) was chosen as the solution of Eq. (4). Finally, based on the analysis performed above the stiffness of the Pasternak foundation by using Eqs. (6) and (8) is

$$k_G = 2.04 bh \sqrt{E_{11} E_{33}}, \quad (61)$$

while for isotropic materials $k_G = 2.04 bh E_{11}$. It is important to note that in most of the works the Pasternak foundation stiffness is related to the shear modulus (Omurtag and Kadıoğlu, 1998; Khazanovich, 2003). It is also noteworthy that in our last work ω was estimated to be 1/2 (Szekrényes and Uj, 2006).

3. Application to delamination specimens

In this section the models of the SCB, SLB and MMB delamination specimens are utilized in order to demonstrate the accuracy of the improved model. For the geometry of the delamination coupons refer to Szekrényes and Uj (2006).

For the SCB specimen we may write that: $M_1 = 0$, $M_2 = Pa$. From Eq. (49) it follows that $M_{\text{I}} = -M_{\text{II}} = -Pa/2$. Comparing the latter to Eq. (50) we may write that $f_{\text{I}} = -f_{\text{II}} = -1/2$ and $a^{\#} = a$. The compliance of the SCB specimen based on Eq. (57) (where the terms C_{EB} and C_{TIM} were determined by following the way shown for example by Ozdil et al. (1998)) becomes ($\omega = 2.5$):

$$C^{\text{SCB}} = \frac{7a^3 + L^3}{2bh^3 E_{11}} + \frac{a + L}{2bhkG_{13}}$$
$$+ \frac{a^3}{2bh^3 E_{11}} \left[f_{\text{W1}} + \frac{f_{\text{SV}}}{2} + f_{\text{SH1}} \right] + \frac{3L^2}{2\pi bh^2 E_{11}} \left(\frac{E_{11}}{G_{13}}\right)^{\frac{1}{2}}. \quad (62)$$

Also, the S–V effect at the clamped end should be considered, i.e. Eq. (26) is also included in the

second term of Eq. (62). The ERRs of the SCB coupon may be obtained from Eq. (48):

$$G_I^{SCB} = \frac{12P^2a^2}{4b^2h^3E_{11}} \left[1 + 0.85\left(\frac{h}{a}\right)\left(\frac{E_{11}}{E_{33}}\right)^{\frac{1}{4}} \right.$$
$$+ 0.71\left(\frac{h}{a}\right)^2\left(\frac{E_{11}}{E_{33}}\right)^{\frac{1}{2}} + 0.32\left(\frac{h}{a}\right)\left(\frac{E_{11}}{G_{13}}\right)^{\frac{1}{2}}$$
$$\left. + 0.1\left(\frac{h}{a}\right)^2\left(\frac{E_{11}}{G_{13}}\right) \right], \tag{63}$$

$$G_{II}^{SCB} = \frac{9P^2a^2}{4b^2h^3E_{11}} \left[1 + 0.22\left(\frac{h}{a}\right)\left(\frac{E_{11}}{G_{13}}\right)^{\frac{1}{2}} + 0.048\left(\frac{h}{a}\right)^2\left(\frac{E_{11}}{G_{13}}\right) \right].$$

The compliance terms, C_{EB} and C_{TIM} of the SLB specimen are given in Szekrényes and Uj, 2004) Furthermore, we may write for the SLB specimen that $M_1 = Pa/2$, $M_2 = 0$. From Eq. (49) it follows that $M_I = M_{II} = Pa/4$. Comparing the latter to Eq. (50) we obtain that $f_I = f_{II} = 1/4$ and $a^{\#} = a$. The compliance of the SLB specimen by using Eq. (57) is (note that C_{SV} in Eq. (57) is excluded)

$$C^{SLB} = \frac{7a^3 + 2L^3}{8bh^3E_{11}} + \frac{a + 2L}{8bhkG_{13}}$$
$$+ \frac{a^3}{8bh^3E_{11}}\left[f_{W1} + \frac{f_{SV}}{2} + f_{SH1}\right]. \tag{64}$$

Using the same mode-I and mode-II bending moments we obtain from Eq. (48) that:

$$G_I^{SLB} = \frac{12P^2a^2}{16b^2h^3E_{11}} \left[1 + 0.85\left(\frac{h}{a}\right)\left(\frac{E_{11}}{E_{33}}\right)^{\frac{1}{4}} \right.$$
$$+ 0.71\left(\frac{h}{a}\right)^2\left(\frac{E_{11}}{E_{33}}\right)^{\frac{1}{2}} + 0.32\left(\frac{h}{a}\right)\left(\frac{E_{11}}{G_{13}}\right)^{\frac{1}{2}}$$
$$\left. + 0.1\left(\frac{h}{a}\right)^2\left(\frac{E_{11}}{G_{13}}\right) \right], \tag{65}$$

$$G_{II}^{SLB} = \frac{9P^2a^2}{16b^2h^3E_{11}} \left[1 + 0.22\left(\frac{h}{a}\right)\left(\frac{E_{11}}{G_{13}}\right)^{\frac{1}{2}} + 0.048\left(\frac{h}{a}\right)^2\left(\frac{E_{11}}{G_{13}}\right) \right].$$

The compliance of the MMB specimen is (Ozdil and Carlsson, 1999b):

$$C^{MMB} = \left(\frac{3c^* - L}{4L}\right)^2 C^{DCB} + \left(1 + \frac{c^*}{L}\right)^2 C^{ENF}, \tag{66}$$

i.e. the solution for the MMB specimen may be obtained by combining the unique solutions for the mode-I DCB (Fig. 4b) and the mode-II ENF (Fig. 4c) specimens. For the former case $P_1 = P$, $P_2 = -P$, while for the latter case $P_1 = P_2 = -P/4$.

Thus, the compliance of the MMB specimen becomes:

$$C^{MMB} = \left(\frac{3c^* - L}{4L}\right)^2\left[\frac{8a^3}{bh^3E_{11}} + \frac{2a^3}{bh^3E_{11}}\left[f_{W1} + f_T + \frac{f_{SV}}{2}\right]\right]$$
$$+ \left(1 + \frac{c^*}{L}\right)^2\left[\frac{3a^3 + 2L^3}{8bh^3E11} + \frac{L}{4bhkG_{13}} + \frac{a^3}{8bh^3E_{11}}f_{SH1}\right], \tag{67}$$

where f_T is given by Eq. (46). Note that Eq. (67) may also be obtained by using Eq. (57). For the MMB specimen: $M_1 = Pc^*a/L$, $M_2 = P(c^* - L)a/2L$, thus we have from Eq. (48):

$$G_I^{MMB} = \frac{12P^2a^2(3c^* - L)^2}{16b^2h^3E_{11}L^2} \left[1 + 0.85\left(\frac{h}{a}\right)\left(\frac{E_{11}}{E_{33}}\right)^{\frac{1}{4}} \right.$$
$$+ 0.71\left(\frac{h}{a}\right)^2\left(\frac{E_{11}}{E_{33}}\right)^{\frac{1}{2}} + 0.32\left(\frac{h}{a}\right)\left(\frac{E_{11}}{G_{13}}\right)^{\frac{1}{2}}$$
$$\left. + 0.1\left(\frac{h}{a}\right)^2\left(\frac{E_{11}}{G_{13}}\right) \right], \tag{68}$$

$$G_{II}^{MMB} = \frac{9P^2a^2(c^* + L)^2}{16b^2h^3E_{11}L^2} \left[1 + 0.22\left(\frac{h}{a}\right)\left(\frac{E_{11}}{G_{13}}\right)^{\frac{1}{2}} \right.$$
$$\left. + 0.048\left(\frac{h}{a}\right)^2\left(\frac{E_{11}}{G_{13}}\right) \right].$$

The mode ratio (G_I/G_{II}) may be obtained by combining the equations above.

4. Finite element solution – VCCT method

For the mixed-mode I/II specimens a series of FE models was developed to obtain the ERRs and the mode ratio in the chosen crack length ranges. For the SCB and SLB specimens the compliance was also computed in order to give some comparison with the analytical solutions. The models were developed in the commercial code COSMOS/M 2.0 using PLANE2D elements under plane stress state. This is consistent with the beam formulation of the problems. The details of the specimens and FE models are shown in a previous work (Szekrényes and Uj, 2006). The models were 150 mm long, $b = 20$ mm wide and $2h = 6.1$ mm thick. For the computation the material properties of a glass/polyester composite is adopted (Szekrényes and Uj, 2004): $E_{11} = 33$ GPa, $E_{33} = 7.2$ GPa, $G_{13} = 3$ GPa and $v_{13} = v_{31} = 0.27$. The formulae of the VCCT method used for the calculation are given by Szekrényes and Uj (2006). A finite element mesh around the crack tip, as suggested by Davidson

and Sundararaman (1996) was constructed. The S–V effect at the clamped end of the SCB specimen was also accounted for. Also, the case of the traditional clamped end was studied in this case. Crack tip elements with finite crack extension of $\Delta a = 0.025$ mm were constructed.

5. Other solutions

Apart from the present model (beam theory-based solution I.) three other solutions are extended for the mentioned fracture specimens: beam theory-based solution II. (Carlsson et al., 1986; Williams, 1989; Olsson, 1992) (denoted as Carlsson–Olsson), a solution based on refined plate theory (Bruno and Greco, 2001a,b) and a numerical (FE) solution by Bao et al. (1992). For the ERR expressions of these solutions refer to Szekrényes and Uj (2006).

6. Results

In the following the compliance and ERR expressions from different solutions are compared to each other. In the work of Bao et al. (1992) expressions for the compliance are not given, and so, this void was addressed by our FE models, except in the case of the MMB specimen, where due to the complex fixture the compliance calculation is difficult. The other two solutions for the compliance of the specimens are detailed in relevant papers (Carlsson et al., 1986; Williams, 1989; Olsson, 1992; Bruno and Greco, 2001a,b). All of the equations were normalized with the results of the Euler–Bernoulli (C_{EB}) beam theory. These are the first terms in Eqs. (62)–(69). The normalized compliance and ERR expressions are plotted against the normalized crack length.

6.1. Compliance

The normalized compliance expressions for the SCB coupon are shown in Fig. 8a. Without the S–V effect the solutions agree well. The FE solution provides somewhat different values compared to the analytically obtained curves if the S–V effect is included. It should be mentioned that the contribution from the S–V effect (the second term in Eq. (62)) at the clamped end of the SCB specimen is about half time of that predicted by the FE model. In fact all of the analytical curves follow the same trend. Quite similar curves were obtained in the case of the SLB specimen, as it is shown in Fig. 8b. For the MMB specimen the normalized compliance was

displayed at four different positions of the load, (c^*) by three different solutions (refer to Fig. 9). In the case of $c^* = 30$ mm the present solution provides the largest improvement. If $c^* = 60$ mm the present and Carlsson–Olsson's solution show similar tendencies. At the other values of c^* the solution by Carlsson–Olsson gives the largest improvement.

6.2. Energy release rate

6.2.1. G_I and G_{II}

The results for the ERR of the SLB and MMB specimens are illustrated in Fig. 10 (for the SCB specimen the same results were obtained for $L = 150$ mm). For the glass/polyester specimens (Fig. 10a) our solution gives the best correlation compared to the numerical solution. The overprediction by Carlsson–Olsson in comparison with Bao's solution is somewhat surprising. Fig 10a also contains the result of the present solution if $\omega = 0$. In this case the difference between the present solution and the one by Carlsson–Olsson is proportional to the difference between the classical elastic foundation model for a pure mode-I problem by Williams (1989) and Eq. (60), i.e. the solution based on the Winkler foundation model for a general mixed-mode I/II problem.

The normalized mode-II component is plotted in Fig. 10b and in each case, the agreement was excellent between our model and the one by Bao et al. (1992). In contrast, the mode-II component is equivalent to the formula of Euler–Bernoulli beam model in accordance with Bruno and Greco (Fig. 10b). Although the model by Carlsson et al. (1986) provides some correction for the mode-II component, it is clear, that our solution (Wang and Qiao, 2004a) is more reasonable.

The results in Fig. 11 confirm the accuracy of the model even for a high modulus carbon/peek composite material (taken from Hashemi et al., 1990a).

6.2.2. The mode ratio

The mode ratios for the SCB specimen by five different approximations are compiled in Fig. 12a. The models by Bruno and Greco and Carlsson–Olsson show the largest mode-I dominance compared to the other solutions. Bao's numerical formulation shows good agreement with our results. Finally, the plane stress FE model also shows some crack length dependence of the mode ratio, although the mode-I dominance is not as significant here as in any of the former cases. The reason for the poor agreement
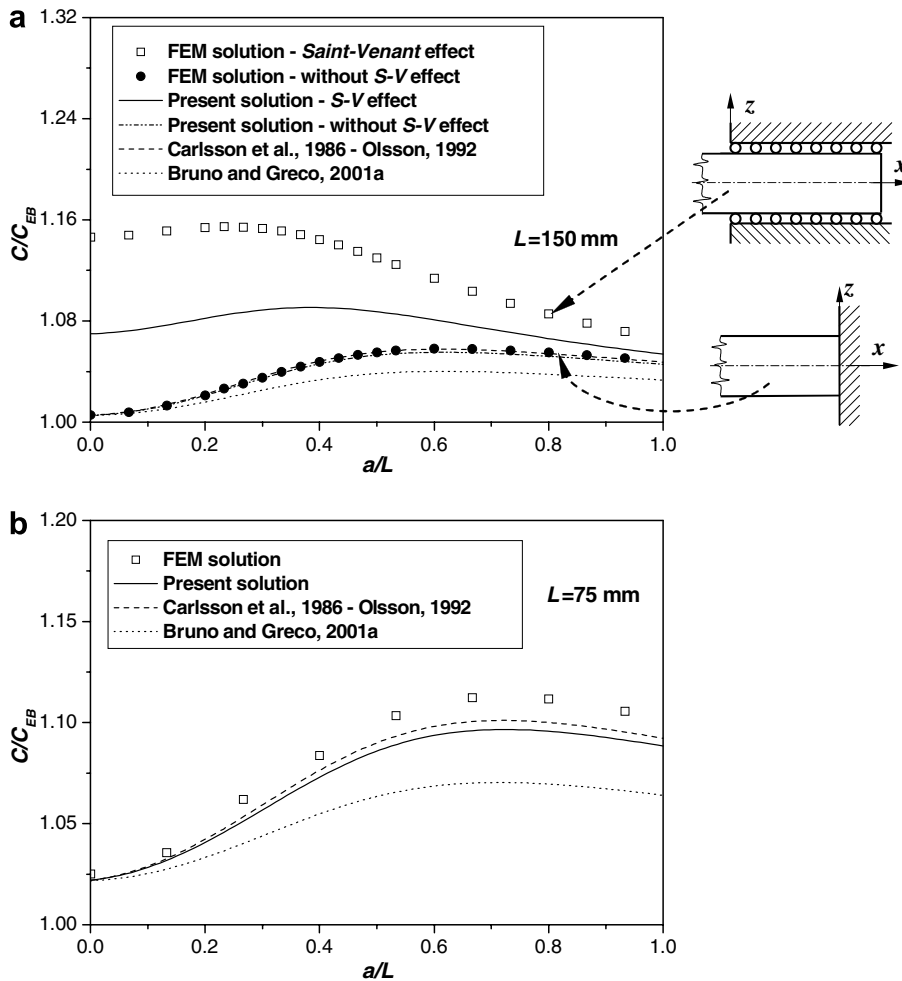
Fig. 8. Comparison of the compliance of the SCB (a) and SLB (b) specimens.

between the results of the VCCT and the other solutions was elaborated by Szekrényes and Uj (2007).

In the case of the SLB specimen the same results were obtained, the only differences are that the half span length is $L = 75$ mm and that the results of the VCCT (Szekrényes and Uj, 2006) agree better with the analysis results than in the SCB specimen.

In Fig. 12b the mode ratios are depicted for the MMB specimen at $c^* = 60$ mm. Essentially the same trends were observed as those in Fig. 12a, although the VCCT agrees better with the analytical methods in this case. Furthermore the results are independent of c^*. For more details refer to Szekrényes and Uj (2006).

6.2.3. The total energy release rate

Finally we investigate the total ERR $(G_1 + G_{11})$ by the four improved solutions in comparison with

the simple beam theory. The results for the SLB and the SCB specimens are collected in Table 1. The solution for the SLB specimen is given in the crack length range of $a = 20–70$ mm, while for the SCB specimen the whole range ($a = 20–100$ mm) is valid. The differences are not significant, but it may be observed that in this respect the solution by Bruno and Greco produces the smallest improvement. Further consequences may be drawn by focusing our attention in Table 2, where the results are listed for the MMB specimen at four different values of the position of the load. If $c^* = 30$ and 60 mm then our and Bao's solution seems to be the best. The other two solutions provide poor results, which may be explained by the fact that in this case there is a mode-II dominated condition. Increasing c^* the mode-I component becomes more and more dominant; therefore the difference between the other
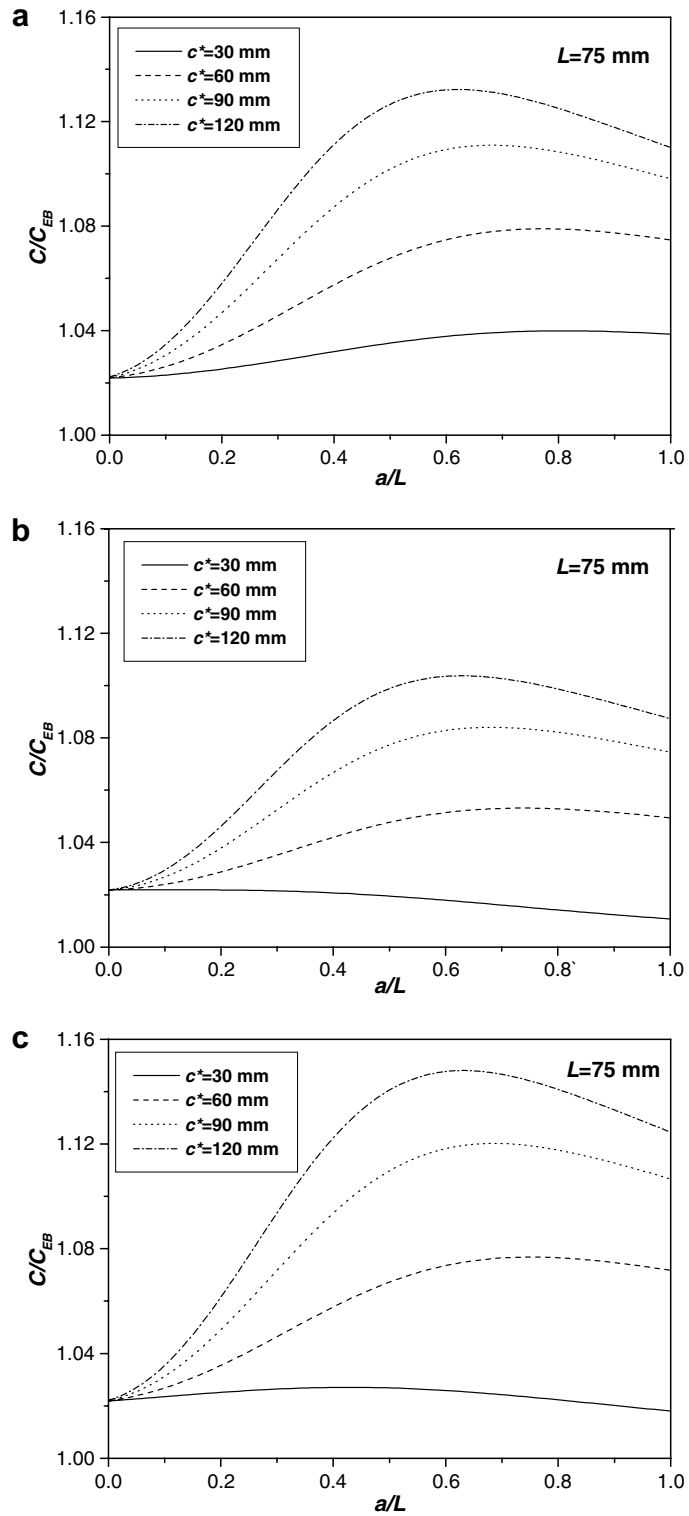
Fig. 9. Comparison of the compliance of the MMB specimen. Present solution (a), solution by Bruno and Greco (2001) (b), and solution by Carlsson et al., 1986 – Olsson, 1992 (c).

solutions and the one by Bao et al. subsequently decays.

7. Discussion

As a consequence, the different solutions give distinct results, which should be clarified. According to the present formulation the total ERR was obtained by a superposition scheme, which incorporates the influence of W–P foundation, S–V effect, transverse shear and CTSD. Interaction among them was not considered, but the mode-I and mode-II ERR components are equally supported by reasonable values. Moreover, the comparison showed that the relation-

ship of our solution to the one by Bao et al. is similar in all the presented cases.

We may assume that Bao's numerical model provides the more accurate result. Their model incorporates all of the former effects and the possible interaction among them. In spite of that we can also state that the form of the formulae is the most difficult in this case. For example the analytical solution showed that the transverse elastic modulus, E_{33} has not any influence on the mode-II ERR (refer to e.g. Eq. (48)), in contrast it is included in Bao et al.'s solution (Bao et al., 1992). This issue was also addressed by Qiao et al. (2003) and they have reported the same conclusion.
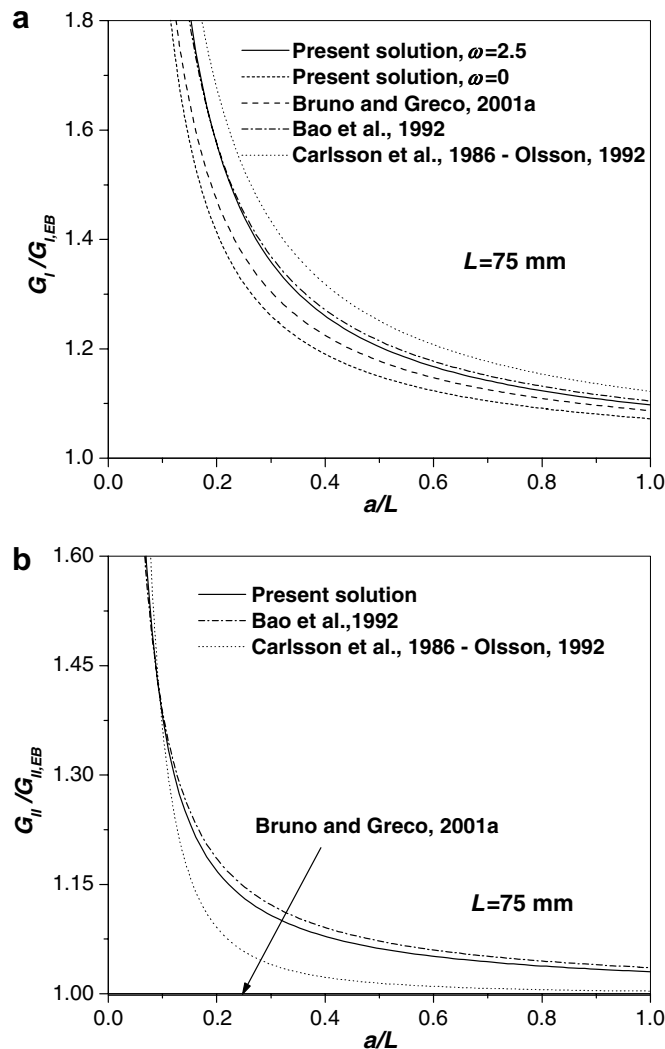

Fig. 10. Comparison of the mode-I (a) and mode-II (b) energy release rates for the SLB and MMB specimens.
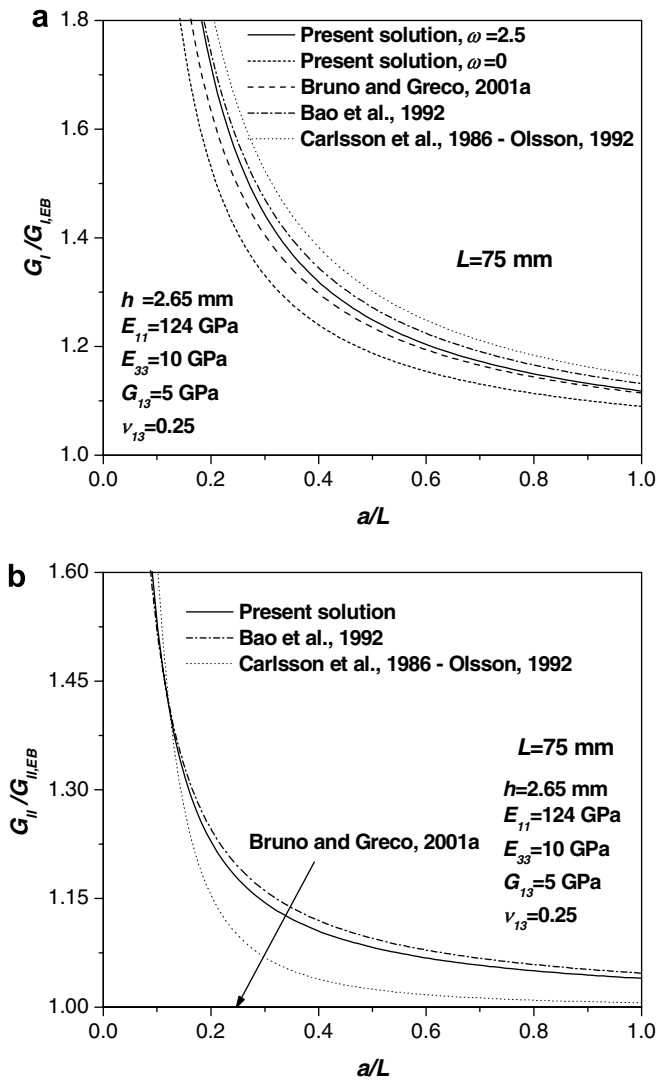
Fig. 11. Comparison of the mode-I (a) and mode-II (b) energy release rates for carbon/PEEK SLB and MMB specimens.

The refined plate model by Bruno and Greco affirms the significance of bending–shear interaction. Their model does not provide improved solution for the mode-II component, while the present and Bao's solutions show that the mode-II component should be contributed apart from simple beam theory. Thus, the overestimated mode ratios may be explained by the lack of correction for the mode-II component. Furthermore the solution does not depend on the through-thickness modulus (E_{33}) of the specimens, it depends only on the shear modulus (G_{13}).

The combined solution by Carlsson and Olsson is based on similar considerations to those of the present beam model. In Section 2 the elastic foundation effect was captured based on a general loading scheme under mixed-mode I/II condition, where the theorem of parallel axes was considered. Apparently, this effect was ignored in Olsson's (Williams') solution, the model does not account for the theorem of parallel axes in the case of the elastic foundation and so it causes the discrepancy between Williams' classical solution and Eq. (60) (if $\omega = 0$). Consequently, the generalization of Williams' solution, which was applied by numerous authors (Reeder and Crews, 1990; Ozdil and Carlsson, 1999b; Chen et al., 1999) for mixed-mode I/II coupons is not straightforward. Apart from that, the mode-II component by Carlsson et al. is only slightly contributed in comparison with the present (Wang and Qiao, 2004a) and Bao's solution. This may cause again the overprediction of the mode ratio.
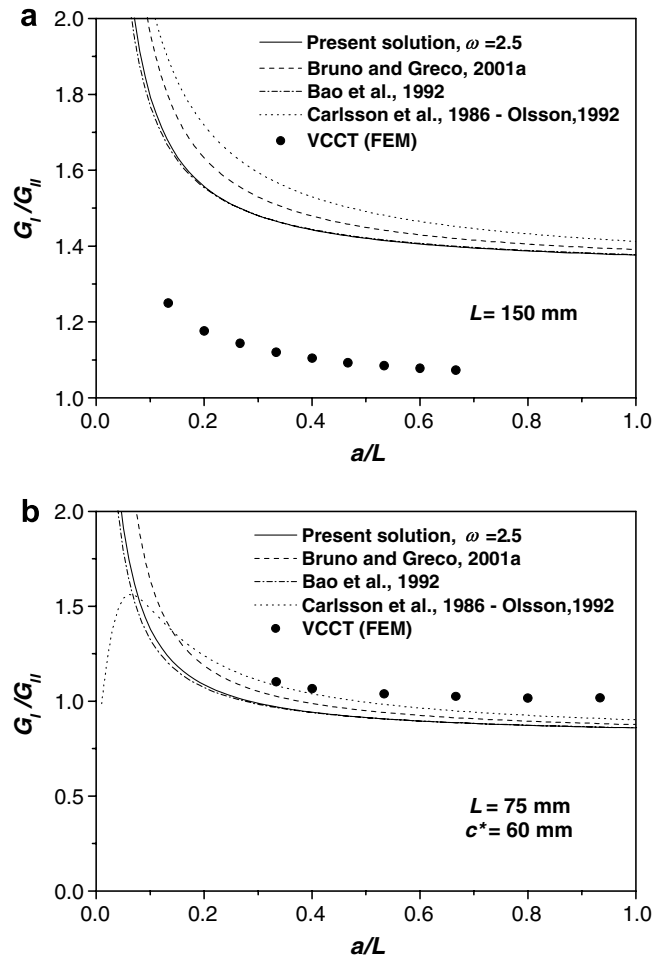
Fig. 12. Comparison of the mode-ratio of the SCB (a) and MMB (b) specimens.

8. Interactions

The interaction among the different mechanical effects and deformations was not considered in the present model and the factors were superimposed rather mechanically. In spite of that in each case the agreement with the most accurate model by Bao et al. (1992) was found to be excellent. In the followings – considering the possible interaction from factor by factor – some justifications are given to explain the reasons for that.

Table 1
Comparison of the total ERR ($G_{I/II}/G_{I/II,EB}$) by different methods, SLB and SCB specimens

a (mm)								
20	30	40	50	60	70	80	90	100
1.287	1.183	1.134	1.105	1.087	1.074	1.064	1.057	1.051[a]
1.197	1.128	1.095	1.075	1.063	1.053	1.047	1.041	1.037[b]
1.301	1.196	1.145	1.115	1.095	1.081	1.071	1.063	1.057[c]
1.303	1.192	1.140	1.110	1.090	1.077	1.067	1.059	1.053[d]

[a] Present.
[b] Bruno and Greco (2001a,b).
[c] Bao et al. (1992).
[d] Carlsson et al. (1986) and Olsson (1992).

Table 2
Comparison of the total ERR ($G_{I/II}/G_{I/II, EB}$) by different methods, MMB specimen

	a (mm)					
	25	30	40	50	60	70
$c^* = 30$ mm	1.102	1.084	1.062	1.049	1.040	1.034[a]
	1.007	1.006	1.004	1.003	1.003	1.002[b]
	1.116	1.097	1.072	1.057	1.048	1.041[c]
	1.042	1.031	1.019	1.013	1.010	1.008[d]
$c^* = 60$ mm	1.196	1.160	1.117	1.092	1.076	1.065[a]
	1.121	1.100	1.074	1.059	1.049	1.042[b]
	1.203	1.168	1.124	1.099	1.082	1.070[c]
	1.191	1.155	1.112	1.088	1.072	1.061[d]
$c^* = 90$ mm	1.241	1.197	1.144	1.114	1.094	1.080[a]
	1.177	1.146	1.108	1.086	1.071	1.061[b]
	1.247	1.204	1.151	1.120	1.099	1.085[c]
	1.263	1.215	1.157	1.124	1.102	1.087[d]
$c^* = 120$ mm	1.261	1.214	1.156	1.123	1.101	1.086[a]
	1.201	1.166	1.123	1.097	1.081	1.069[b]
	1.267	1.220	1.163	1.129	1.107	1.091[c]
	1.295	1.241	1.177	1.140	1.115	1.098[d]

[a] Present.
[b] Bruno and Greco (2001a,b).
[c] Bao et al. (1992).
[d] Carlsson et al. (1986), Olsson (1992).

8.1. Winkler–Pasternak foundation and crack tip shear deformation

It can be seen that the CTSD causes an increment in the deflection of both the upper and lower beam elements. However, in each case the increment of the deflection acts always in the same direction, i.e. the deflection functions are equal to each other. Using Eq. (39) the effect of the CTSD could be included in the functional in Eq. (1), although it is now obvious that it would influence neither the governing equations (Eq. (2)) nor the results. This indicates that the increment of the deflection from CTSD does not cause interaction with the two-parameter foundation.

8.2. Winkler–Pasternak foundation and Saint–Venant effect

The S–V effect induces the rotation of the cross section of the crack tip; however it does not cause changes in the deflection functions. So, if only the cross section rotates then the deflection in the uncracked region holds its original shape. Since the two-parameter foundation model incorporates

the differences in the deflection and its derivative it is elaborated that there is probably no interaction between these effects.

8.3. Crack tip shear deformation and Saint–Venant effect

The S–V effect involves strain compatibility along the interface. So, in a mixed-mode I/II problem the rotation of the cross sections of the upper and lower beam elements at the crack tip induces axial displacements in the same direction, and so they do not increase or decrease the shear stress at the interface. This confirms that there is no interaction.

8.4. Crack tip shear deformation and transverse shear

In accordance with the model utilized in the analysis (Section 2.4) the shear tractions are considered as the results of the external loading, i.e. the effect of transverse shear is included in the loading. Otherwise the combination of Timoshenko beam theory with the theory of CTSD leads to the same governing equation as Eq. (35). So, interaction between CTSD and transverse shear does not take place.

8.5. Saint–Venant effect and transverse shear

The model of S–V effect assumes zero vertical displacements at the crack tip and in the clamped end. To calculate the rotation of the cross section we applied Castigliano's second theorem, which involves the derivative of the strain energy with respect to the bending moment. Although the effect of transverse shear can be included in the strain energy (Eq. (18)) due to the differentiation with respect to the bending moment it vanishes. This indicates that there is not any interaction.

8.6. Winkler–Pasternak foundation and transverse shear

These are the only effects, where interaction may arise. However the solution of the problem is quite difficult and involves very complicated solution functions. The form of the simplified correction function (Eqs. (11) and (14)) would be much more complicated, which would make the application of Eq. (48) more difficult. On the other hand the interaction between these two factors is estimated to be very small, because the transverse shear causes only a small amount of deformation.

9. Conclusions

This work presented an improved solution for the compliance and energy release rate of symmetric, slender and orthotropic unidirectional composite delamination specimens. The problem was investigated based on a general loading scheme including the following effects apart from Euler–Bernoulli beam theory: Winkler–Pasternak foundation, transverse shear, Saint–Venant effect and crack tip shear deformation. These theories were used to obtain the solution for the compliance and the energy release rate based on a generalized mixed-mode I/II problem and the results were implemented into Williams' global mode decomposition method. It was shown that the first three of these effects contribute only to the mode-I energy release rate, while the crack tip shear deformation improves only the mode-II component. Also, a general expression for the compliance of unidirectional composite beams with midplane delamination was developed, however the determination of the terms related to the Euler–Bernoulli and Timoshenko beam theory – depending on the geometry of the problem – requires a unique analysis. Finally, the coefficient, ω and the stiffness of the Pasternak foundation was determined using the developed model and the finite element method. Perhaps, this can be applied also for dynamic problems. The performed analysis helps us to understand better the different mechanism and processes, which take place during the delamination.

The possible interactions among the mentioned effects were not accounted for, but it was elaborated that interaction probably may arise only between the Winkler–Pasternak foundation and transverse shear.

Three other solutions were utilised for comparison with the one developed in this work. The most important conclusion of the comparison is that the present solution shows the same relation to the numerical model by Bao et al. in all the presented cases.

Acknowledgements

Appendix A

The results of the FE calculations for the determination of ω are given in Table A1.

Table A1
Corrections for the ERR of the DCB specimen from Winkler–Pasternak elastic foundation if $G_13 = 100\,000$ GPa and $\omega = 2.5$

		a (mm)							
		30	40	50	60	70	80	90	100
E-glass/polyester specimen: $E_{11} = 33$ GPa, $E_{33} = 7.2$ Pa, $v_{13} = 0.27$ (present)									
$h = 2$ mm	$G_{I,FEM}/G_{I,EB}$	1.090	1.067	1.053	1.047	1.041	1.035	1.031	1.028
	$G_{I,WP}/G_{I,EB}$	1.089	1.066	1.052	1.043	1.037	1.032	1.028	1.025
	Difference (%)	0.092	0.094	0.095	0.382	0.384	0.289	0.291	0.292
$h = 3.05$ mm	$G_{I,FEM}/G_{I,EB}$	1.143	1.106	1.084	1.070	1.060	1.052	1.046	1.042
	$G_{I,WP}/G_{I,EB}$	1.142	1.103	1.081	1.067	1.057	1.049	1.043	1.039
	Difference (%)	0.087	0.271	0.276	0.280	0.283	0.285	0.287	0.288
$h = 4.5$ mm	$G_{I,FEM}/G_{I,EB}$	1.218	1.161	1.128	1.106	1.090	1.079	1.070	1.063
	$G_{I,WP}/G_{I,EB}$	1.219	1.158	1.123	1.101	1.086	1.074	1.066	1.059
	Difference (%)	−0.082	0.258	0.443	0.452	0.357	0.463	0.373	0.376
Carbon/epoxy specimen: $E_{11} = 124$ GPa, $E_{33} = 10$ GPa, $v_{13} = 0.25$ (Hashemi et al., 1990a)									
$h = 2$ mm	$G_{I,FEM}/G_{I,EB}$	1.124	1.092	1.073	1.066	1.057	1.050	1.044	1.040
	$G_{I,WP}/G_{I,EB}$	1.117	1.086	1.067	1.056	1.047	1.041	1.036	1.033
	Difference (%)	0.062	0.549	0.559	0.938	0.946	0.854	0.766	0.673
$h = 3.05$ mm	$G_{I,FEM}/G_{I,EB}$	1.192	1.142	1.113	1.094	1.080	1.070	1.062	1.056
	$G_{I,WP}/G_{I,EB}$	1.187	1.135	1.106	1.087	1.074	1.064	1.057	1.051
	Difference (%)	0.419	0.613	0.628	0.640	0.574	0.561	0.471	0.473

Table A1 (*continued*)

		a (mm)							
		30	40	50	60	70	80	90	100
$h = 4.5$ mm	$G_{I,FEM}/G_{I,EB}$	1.291	1.213	1.169	1.140	1.119	1.104	1.092	1.083
	$G_{I,WP}/G_{I,EB}$	1.294	1.210	1.163	1.133	1.112	1.097	1.086	1.076
	Difference (%)	−0.232	0.247	0.513	0.614	0.656	0.634	0.549	0.646
Isotropic specimen: $E_{11} = 33$ GPa, $E_{33} = 33$ GPa, $v_{13} = 0.27$									
$h = 2$ mm	$G_{I,FEM}/G_{I,EB}$	1.058	1.044	1.035	1.030	1.026	1.023	1.020	1.018
	$G_{I,WP}/G_{I,EB}$	1.059	1.044	1.035	1.029	1.025	1.022	1.019	1.017
	Difference (%)	−0.095	0.000	0.000	0.097	0.097	0.098	0.098	0.098
$h = 3.05$ mm	$G_{I,FEM}/G_{I,EB}$	1.091	1.068	1.054	1.045	1.038	1.034	1.030	1.027
	$G_{I,WP}/G_{I,EB}$	1.093	1.068	1.054	1.045	1.038	1.033	1.029	1.026
	Difference (%)	−0.183	0.000	0.000	0.000	0.000	0.097	0.097	0.097
$h = 4.5$ mm	$G_{I,FEM}/G_{I,EB}$	1.137	1.102	1.081	1.067	1.057	1.050	1.045	1.040
	$G_{I,WP}/G_{I,EB}$	1.143	1.104	1.082	1.067	1.057	1.050	1.044	1.039
	Difference (%)	−0.528	−0.181	−0.093	0.000	0.000	0.000	0.096	0.096

$G_{I,EB}$ – solution based on Euler–Bernoulli beam theory.
$G_{I,FEM}$ – plane stress FE model, second in Eq. (58), $G_{I,WP}$ – analytical solution, Eq. (60).

References

Anderson, T.L., 2005. Fracture Mechanics – Fundamentals and Applications, third ed. CRC Press, Taylor & Francis Group, Boca Raton, London, New York, Singapore.

Alemdar, B.N., Gülkan, P., 1997. Beams on generalized foundations: supplementary element matrices. Engineering Structures 19, 910–920.

Bao, G., Ho, S., Suo, Z., Fan, B., 1992. The role of material orthotropy in fracture specimens for composites. International Journal of Solids and Structures 29, 1105–1116.

Bruno, D., Greco, F., 2001a. Mixed mode delamination in plates: a refined approach. International Journal of Solids and Structures 38, 9149–9177.

Bruno, D., Greco, F., 2001b. Delamination in composite plates: influence of shear deformability on interfacial debonding. Cement & Concrete Composites 23, 33–45.

Carlsson, L.A., Gillespie, J.W., Pipes, R.B., 1986. On the analysis and design of the end notched flexure (ENF) specimen for mode II testing. Journal of Composite Materials 20, 594–604.

Chen, J.H., Sernow, R., Schulz, G., Hinrichsen, G., 1999. A modification of the mixed-mode bending test apparatus. Composites Part A: Applied Science and Manufacturing 30, 871–877.

Coşkun, İ., 2003. The response of a finite beam on a tensionless Pasternak foundation subjected to a harmonic load. European Journal of Mechanics 22, 151–161.

Crews, Jr., J.H., Reeder, J.R., 1988. A mixed-mode bending apparatus for delamination testing. NASA Technical Memorandum 100662, August, pp. 1–37

Davidson, B.D., Sundararaman, V., 1996. A single leg bending test for interfacial fracture toughness determination. International Journal of Fracture 78, 193–210.

Ding, W., Kortschot, M.T., 1999. A simplified beam analysis of the end notched flexure mode II delamination specimen. Composite Structures 45, 271–278.

Ducept, F., Gamby, D., Davies, P., 1999. A mixed-mode failure criterion derived from tests of symmetric and asymmetric specimens. Composites Science and Technology 59, 609–619.

Filipich, C.P., Rosales, M.B., 2002. A further study about the behaviour of foundation plies and beams in a Winkler–Pasternak soil. International Journal of Mechanical Sciences 44, 21–36.

Hashemi, S., Kinloch, J., Williams, J.G., 1990a. The effects of geometry, rate and temperature on mode I, mode II and mixed-mode I/II interlaminar fracture toughness of carbon-fibre/poly(ether–ether ketone) composites. Journal of Composite Materials 24, 918–956.

Hashemi, S., Kinloch, J., Williams, J.G., 1990b. Mechanics and mechanisms of delamination in a poly(ether sulphone)-fibre composites. Composites Science and Technology 7, 429–462.

Hutchinson, J.W., Suo, Z., 1992. Mixed mode cracking in layered materials. In: Advances in Applied Mechanics. Academic Press, New York, pp. 63–191.

Kanninen, M.F., Popelar, C.H., 1985. Advanced Fracture Mechanics. Oxford University Press, New York.

Khazanovich, L. (2003). Finite element analysis of curling of slabs on Pasternak foundation. In: 16th ASCE Engineering Mechanics Conference, July 16–18, University of Washington, Seattle.

Lai, Y.H., Rakestraw, M.D., Dillard, D.A., 1996. The cracked lap shear specimen revisited – a closed form solution. International Journal of Solids and Structures 33, 1725–1743.

Olsson, R., 1992. A simplified improved beam analysis of the DCB specimen. Composites Science and Technology 43, 329–338.

Omurtag, M.H., Kadıoğlu, F., 1998. Free vibration analysis of orthotropic plates resting on Pasternak foundation by mixed finite element formulation. Computers and Structures 67, 253–265.

Ozdil, F., Carlsson, L.A., Davies, P., 1998. Beam analysis of angle-ply laminate end-notched flexure specimens. Composites Science and Technology 58, 1929–1938.

Ozdil, F., Carlsson, L.A., 1999a. Beam analysis of angle-ply laminate DCB specimens. Composites Science and Technology 59, 305–315.

Ozdil, F., Carlsson, L.A., 1999b. Beam analysis of angle-ply laminate mixed-mode bending specimens. Composites Science and Technology 59, 937–945.

Qiao, P., Wang, J., Davalos, J.F., 2003. Analysis of tapered ENF specimen and characterization of bonded interface fracture under mode-II loading. International Journal of Solids and Structures 40, 1865–1884.

Raju, I.S., Crews Jr., J.H., Aminpour, M.A., 1988. Convergence of strain energy release rate components for edge-delaminated composite laminates. Engineering Fracture Mechanics 30, 383–439.

Reeder, J.R., Crews, J.R., 1990. Mixed-mode bending method for delamination testing. AIAA Journal 28, 1270–1276.

Reyes, G., Cantwell, W.J., 2000. The mechanical properties of fibre–metal laminates based on glass fibre reinforced polypropylene. Composites Science and Technology 60, 1085–1094.

Rybicki, E.F., Kanninen, M.F., 1977. A finite element calculation of stress intensity factors by a modified crack closure integral. Engineering Fracture Mechanics 9, 931–938.

Sheinman, I., Kardomateas, G.A., 1997. Energy release rate and stress intensity factors for delaminated composite laminates. International Journal of Solids and Structures 34, 451–459.

Rosa, De M.A., 1995. Free vibrations of Timoshenko beams on two-parameter elastic foundation. Computers & Structures 57, 151–156.

Sundararaman, V., Davidson, B.D., 1997. An unsymmetric double cantilever beam test for interfacial fracture toughness determination. International Journal of Solids and Structures 34, 799–817.

Sundararaman, V., Davidson, B.D., 1998. An unsymmetric end-notched flexure test for interfacial fracture toughness determination. Engineering Fracture Mechanics 60, 361–377.

Suo, Z., Hutchinson, J.W., 1990. Interface crack between two elastic layers. International Journal of Fracture 43, 1–18.

Suo, Z., 1990. Delamination specimens for orthotropic materials. Journal of Applied Mechanics 57, 627–634.

Szekrényes, A., Uj, J., 2004. Beam and finite element analysis of quasi-unidirectional SLB and ELS specimens. Composites Science and Technology 64, 2393–2406.

Szekrényes, A., Uj, J., 2005. Mode-II fracture in E-glass/polyester composite. Journal of Composite Materials 39, 1747–1768.

Szekrényes, A. 2005. Delamination of Composite Specimens. Ph.D. Thesis, Budapest University of Technology and Economics, Faculty of Mechanical Engineering, Department of Applied Mechanics, Budapest, PhD-261/2004.

Szekrényes, A., Uj, J., 2006. Comparison of some improved solutions for mixed-mode composite delamination coupons. Composite Structures (72/3), 321–329.

Szekrényes, A., Uj, J., 2007. Over-leg bending test for mixed-mode I/II interlaminar fracture in composite laminates. International Journal of Damage Mechanics (16/1), 5–33.

Wang, J., Qiao, P., 2004a. Novel beam analysis of the end notched flexure specimen for mode-II fracture. Engineering Fracture Mechanics 71, 219–231.

Wang, J., Qiao, P., 2004b. On the energy release rate and mode mix of delaminated shear deformable composite plates. International Journal of Solids and Structures 41, 2757–2779.

Wang, J., Qiao, P., 2004c. Interface crack between two shear deformable elastic layers. Journal of the Mechanics and Physics of Solids 52, 891–905.

Wang, Y., Williams, J.G., 1992. Corrections for mode II fracture toughness specimens of composite materials. Composites Science and Technology 43, 251–256.

Washizu, K., 1968. Variational Methods in Elasticity and Plasticity. Pergamon Press, Headington Hill Hall, Oxford, London.

Williams, J.G., 1988. On the calculation of energy release rates for cracked laminates. International Journal of Fracture 36, 101–119.

Williams, J.G., 1989. End corrections for orthotropic DCB specimens. Composites Science and Technology 35, 367–376.

Zou, Z., Reid, S.R., Soden, P.D., Li, S., 2001. Mode separation of energy release rate for delamination in composite laminates using sublaminates. International Journal of Solids and Structures 38, 2597–2613.

Zou, Z., Reid, S.R., Li, S., Soden, P.D., 2002. Application of a delamination model to laminated composites structures. Composite Structures 56, 375–389.